Synthesis and Properties of Elastomer-Modified Epoxy–Methacrylate Sequential Interpenetrating Networks

J. M. SANDS, R. E. JENSEN, B. K. FINK, S. H. MCKNIGHT

Army Research Laboratory (AMSRL-WM-M), Building 4600 Deer Creek Loop, Aberdeen Proving Ground, Maryland 21005

Received 2 May 2000; accepted 30 May 2000

ABSTRACT: The structure and properties of copolymerized sequential-interpenetrating networks (SeqIPNs) synthesized from amine-cured epoxies and free-radical polymerized dimethacrylates were examined. Materials were synthesized with and without the incorporation of an epoxy-terminated butadiene–nitrile reactive elastomer. Synthesis proceeded through full thermal cure of the epoxy–amine network, followed by polymerization of the methacrylate network. The methacrylate reactions were free-radically induced using thermal (peroxide-initiated) or photochemical [electron-beam (e-beam)] techniques. Fourier transform infrared spectroscopy was used to monitor epoxy–amine step-growth polymerization *in situ* and to measure final cure conversion of methacrylates. Structural examination of the IPNs using atomic force microscopy and scanning electron microscopy revealed microphase separation in the neat–SeqIPN materials and macroscopic phase separation of rubber-rich domains for elastomer-modified networks. Dynamic mechanical analysis of the SeqIPN determined that the properties of the network are strongly dependent on the cure conditions. Furthermore, the viscoelastic behavior of the e-beam–cured SeqIPN could be adequately described by the Williams–Landel–Ferry and Kohrausch–Willams–Watts equations, presumably because of a strong coupling between the epoxy–amine and methacrylate networks. © 2001 John Wiley & Sons, Inc. J Appl Polym Sci 81: 530–545, 2001

Key words: epoxy; methacrylate; interpenetrating polymer networks (IPNs); electron beam

INTRODUCTION

Interpenetrating networks (IPNs) represent a broad category of polymeric materials that offer the ability to control thermal and mechanical properties through materials selection and reaction conditions. IPNs are synthesized by the network polymerization of one or more monomers in the presence of another network.[1] The two networks can be polymerized simultaneously (SimIPN) or sequentially (SeqIPN) to produce desired structures. Networks in IPNs are frequently observed to phase- or microphase-separate during the course of the chemical reactions.[2] The order of the reactions, rate, and the miscibility of the two networks with each other can produce a number of interesting multiphase morphologies and properties.

The ability to select systems and control the polymerization reactions can lead to tailored structures and properties. Independent reaction pathways are often desirable and offer the greatest degree of control in the final IPN. Numerous strategies can be envisioned to provide independent polymerization reactions. In this study, we

Correspondence to: J. Sands.

Contract grant sponsor: Strategic Environmental Research and Development Program (SERDP).

Journal of Applied Polymer Science, Vol. 81, 530–545 (2001)

investigate SeqIPNs formed when epoxy–amine (EA) networks are reacted in the presence of dimethacrylate monomers. During the formation of the epoxy–amine system, the methacrylates remain inert and behave as a diluent. The methacrylates are subsequently polymerized following the preliminary epoxy–amine reactions. The methacrylate polymerization can occur thermally using peroxide initiators, or alternatively, athermally using photochemical methods including ultraviolet or electron-beam (e-beam) irradiation techniques. The selection of the molecular weight, functionality, and reactivity of the starting monomers has been shown to profoundly affect thermomechanical properties in these systems.[3]

Internetwork chemical bonds can be incorporated into the molecular architecture to covalently link the individual interpenetrating networks. This additional network design parameter can significantly alter the thermal and mechanical properties of the final material. This approach has been used to control the properties of epoxy–acrylate and urethane–acrylate IPN systems.[4] It was previously shown that the cure shrinkage, glass-transition temperature (T_g), and viscoelastic properties of epoxy–acrylate coreacted SeqIPN systems are strongly dependent on the degree of coupling between the two networks.[5] Many of these systems also possessed improved modulus and strength. These epoxy–acrylate IPNs have very attractive structural properties and have been used as liquid-molding resins for glass and carbon-reinforced polymer matrix composite (PMC) materials and structural adhesives. Despite these improvements, these resins do not exhibit the necessary toughness that is required in certain PMC and adhesive applications.

Both traditional epoxy and methacrylate networks can be quite brittle, so the improvement in mechanical performance resulting from IPN formation may be insufficient to meet the specific performance requirements for potential adhesive and composite applications. The lack of toughness in traditional epoxy networks has been addressed through the incorporation of reactive liquid rubbers [e.g., epoxy-terminated butadiene nitrile (ETBN)], which phase-separate during cure to yield increased toughness.[6] The enhanced toughness is obtained with minimal negative effects on critical structural properties including modulus and glass-transition temperature. It was demonstrated for epoxy materials that the most effective toughening occurs when phase separation of the rubber domains is nearly complete, such that minimal elastomer remains dissolved in the matrix phase.[7] Macrostructural features, such as the volume fraction, particle size, and interparticle spacing of the rubber-rich domains, strongly affect the ultimate properties of the modified thermoset network.[8]

The incorporation of reactive elastomers into epoxy–methacrylate IPNs may be a suitable method to modify the macrostructure and properties of these materials and was been examined.[9] However, because of the rapid cure rates for e-beam processing, the phase separation of the rubber domains must be achieved during the comparatively slow polymerization of the epoxy–amine network. Additionally, the amount of elastomer that remains in solution should be minimized, to maintain a relatively high T_g upon final cure. The unreacted methacrylate monomers may act as effective ETBN solvents and could hinder phase separation from the growing epoxy–amine network. The composition and reaction conditions that produce desired macrostructures must be studied. In this work, the composition and cure conditions producing two-phase rubber-toughened SeqIPN materials are examined. The polymerization rate for formation of the epoxy–amine network, the macrostructural features, and the thermomechanical properties of the full IPNs are also characterized.

EXPERIMENTAL

Materials

The SeqIPNs synthesized in this work are illustrated schematically in Figure 1. The initial network consists of a thermally cured epoxy–amine network polymerized in the presence of nonreacting dimethacrylate monomers. Additionally, a bifunctional epoxy–methacrylate coupling monomer is reacted into the EA network during the epoxy–amine reaction. The bifunctional coupling monomer (BDGEBA) was synthesized in our laboratory following the procedure outlined by Doyle et al.[10] for reacting diepoxides with methacrylic acid. Based on our earlier results, one-quarter (25%) of the active amine reaction sites are bonded to BDGEBA in the final EA network, providing internetwork molecular crosslink sites. The EA network is fully reacted by thermal processing, producing a swollen gel structure. Next, the methacrylate free-radical polymerization is initiated, either thermally with the

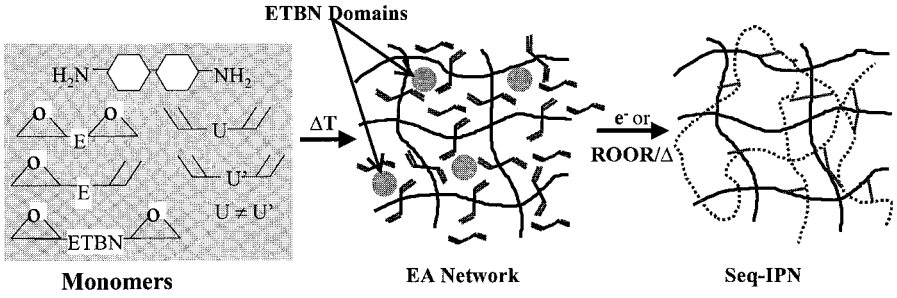

Figure 1 Schematic synthesis of SeqIPN structures.

addition of an organic peroxide (e.g., *t*-butyl peroxide) or photochemically with e-beam irradiation. The dimethacrylates produce a highly crosslinked glassy polymer upon methacrylate curing. In general, the selection of methacrylates and epoxides is variable. For this research, we selected monomers that are suitable for structural applications, such as composite resins and adhesives.

Table I shows the molecular structure and molecular weights of the monomers used to create the SeqIPNs in this study. We selected diglycidyl ether of bisphenol A (DGEBA) epoxides and a cycloaliphatic primary diamine curing agent, bis(*p*-aminocyclohexyl) methane (PACM). The free-radical methacrylate network is composed of two difunctional methacrylates: methacrylated-DGEBA (MDGEBA) and 1,6-hexanediol dimethacrylate (HDDMA). HDDMA was used to control viscosity, add flexibility, and increase tackiness. In all SeqIPNs, the fraction of HDDMA was held constant at 10 wt %. Some SeqIPNs were modified by the addition of an epoxy-terminated butadiene–nitrile rubber (ETBN).

Initially, several compositions were synthesized using the starting materials shown in Table I. Blends of these monomers were thermally

Table I Monomer Structures in SeqIPN Formulations

Identification	Structure	MW
DGEBA	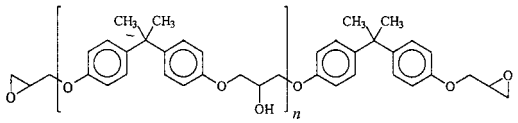	370–384
MDGEBA	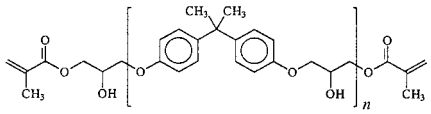	542–554
BDGEBA	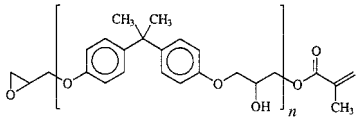	456–470
HDDMA	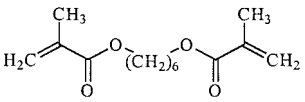	254
ETBN	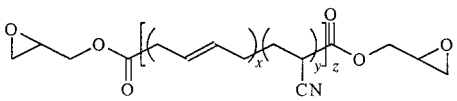	3600–4000 (y = 18%)
PACM	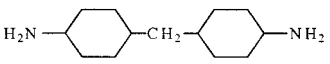	210

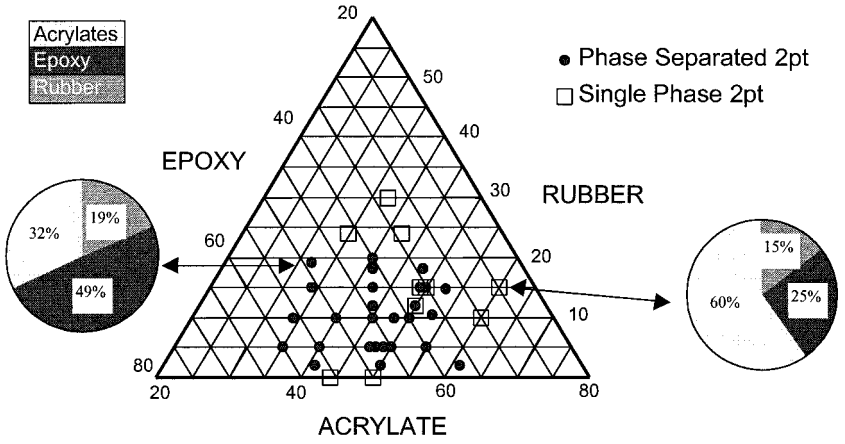

Figure 2 Optical cloud-point determinations for rubber-phase separation in SeqIPN blends.

cured to form a swollen gel and subsequently characterized by T_g and turbidity measurements. Rubber-toughened formulations exhibited strong phase separation over a broad range of network compositions. Figure 2 shows the ternary phase diagram for ETBN-modified SeqIPNs determined from turbidity measurements. The phase envelope in the diagram reveals that in high concentrations, the dimethacrylates (>60 wt %) act as a solvent for the ETBN and suppress formation of rubber-rich domains. Although some specimens are optically transparent, a microheterogeneous morphology may still be present. However, this was not verified because phase separation producing 0.1- to 10.0-μm domains was desired to achieve improved toughness.[11] Additionally, solubilized rubber would diminish the performance expectation for toughened systems, particularly with respect to T_g.

Based on the results of these preliminary formulations, SeqIPN compositions were selected where the two networks are mixed in approximately equal weight fractions (e.g., 50/50), while keeping the concentration of HDDMA at 10 wt %. Two compositions (with and without ETBN) and two cure methods (e-beam and thermal) were chosen to provide insight into the role of cure condition and elastomer modification on the structure and properties of the SeqIPNs. Additionally, the cure behavior and properties of the SeqIPNs are compared to model networks consisting of both ETBN-modified and unmodified epoxy–amine thermosets. These model systems are formulated without diluents and are traditional thermoset epoxy networks. The compositions of the systems described here are listed by weight percentage in Table II.

Characterization Methods

Fourier transform infrared spectroscopy (FTIR) was used to follow polymerization kinetics *in situ*. The FTIR spectra were collected using a Nicolet Magna IR-5DBX spectrophotometer (Nicolet Instruments, Madison, WI) with a KBr beam splitter. Spectra were collected with a resolution of 4

Table II Chemical Compositions of Experimental Resins (wt %)

System	Cure Type	Amine	DGEBA	ETBN	MDGEBA	HDDMA	BDGEBA
I00E	E-beam	9.2	32.9	0	38.8	10	9.1
I01E	E-beam	8.5	30.4	9.7	32.1	10	7.7
I00T	Thermal	9.2	32.9	0	38.8	10	9.1
I01T	Thermal	8.5	30.4	9.7	32.1	10	7.7
E00T	Thermal	22.7	77.3	0	0	0	0
E01T	Thermal	20	70	10	0	0	0

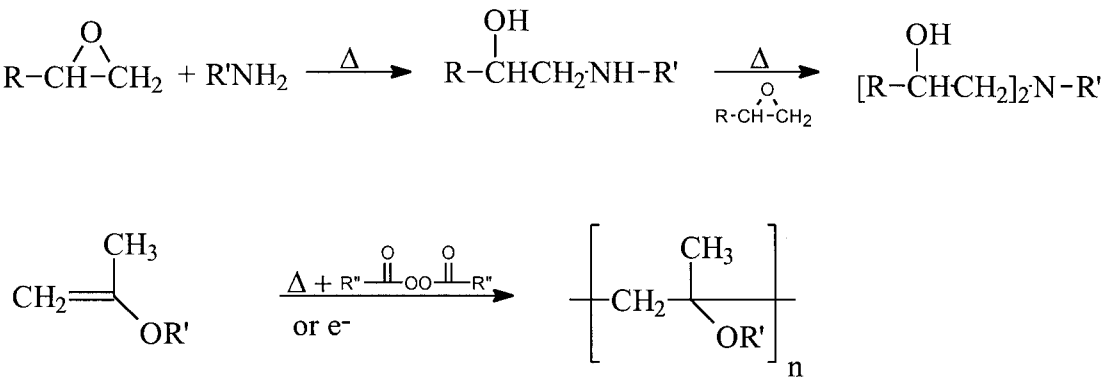

Figure 3 Generalized epoxide and methacrylate homopolymerization products.

cm^{-1} over 32 scans for the frequency range from 4000 to 400 cm^{-1}. Spectral data were collected every 2 min and evaluations of the characteristic vibrational bands were performed using peak–height and peak–area measurement techniques. The infrared vibrational modes of interest for kinetics include the epoxide ring stretch (916 cm^{-1}), the methacrylate C═C symmetric stretch (1637 cm^{-1}), and the methacrylate CH out-of-plane stretch (945 cm^{-1}). Additionally, the *para*-substituted benzene breathing mode (1510 cm^{-1}) was used as the internal standard.

Atomic force microscopy measurements were performed on freeze-fractured specimens using a Digital Instruments Dimension 3000 atomic force microscope (Digital Instruments, Santa Barbara, CA). Fracture surfaces were viewed in the as-fractured condition with no additional etching performed. Imaging was obtained using the tapping mode, which minimizes sample tip interactions that may damage the surface of the polymer. Height and amplitude signals were recorded simultaneously. Postprocessing and analysis of the raw images was performed using the software provided with the instrument. Scanning electron microscopy (SEM) was performed using secondary electron detection on an Amray 1830 (Amray, Bedford, MA) with Kevex (Kevex, Valencia, CA) digital capture. Brittle fracture surfaces of the SeqIPN samples were studied after coating with a 7-nm gold–palladium (Au-Pd) conductive layer. The SEM was operated using a tip voltage of 7.0 kV above the grounded target.

Dynamic mechanical analysis (DMA) was performed using a TA Instruments 2980 DMA (TA Instruments, New Castle, DE) in the dual-cantilever bending mode. The samples were tested using a 20-mm frame and an oscillatory displacement of 7.5 μm. Typical samples were approximately 12 × 1.65 mm (width × thickness), respectively. Single-frequency sweeps were scanned at 1 Hz, from −135 to 225°C at a heating rate of 2.0°C/min. Multiple-frequency sweeps were measured at 0.1, 0.3, 1, 3, 10, and 30 Hz in 3°C isothermal steps. The T_g's were taken as the peak maximum of the loss modulus (E'') curves measured at 1 Hz. All DMA results reported were taken from second-heat measurements.

Differential scanning calorimetry was done using a TA Instruments 2920 MDSC operated in the standard mode at a heating rate of 10°C/min. All scans reported are second-heat values. First-heat residual heats of reaction were negligible (<5 J/g) in all cases.

Network Formation

EA Network Formation

The reaction of epoxide with amine (Fig. 3) proceeds via a traditional ring-opening addition mechanism to form an ether linkage and a secondary alcohol.[12] In the absence of catalysts, the rate of this reaction is primarily dependent on the structure and the concentrations of amine and epoxide as well as the cure temperature. As the polymerization progresses, monomer and polymer diffusion slow dramatically as the molecular weight of the network advances toward vitrification and gelation. The polymerization rate during the early stages is least dependent on diffusional limits and is used to calculate the intrinsic polymerization rate. In the EA reaction of the SeqIPNs, the presence of the methacrylate monomers may affect the curing mechanisms for formation of the EA network. One would predict that the presence of reactive monomers may interfere with the traditional cure mechanisms of EA and either catalyze or hinder the polymerization. A

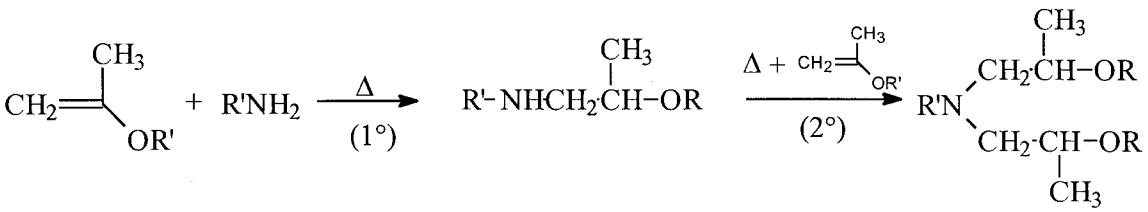

Figure 4 Michael's addition products for reaction with primary (1°) and secondary (2°) amine.

catalyzed polymerization would be reflected by a reduction in the activation energy for formation. Moreover, diluents have been observed to increase cure conversion in polymer network formations,[13] which is attributed to a reduction in diffusional limits or, equivalently, an increase in the vitrification temperature. This secondary impact would be synonymous with improved cure conversions in the EA network of the SeqIPN compared to those in model EA networks, but it would not indicate a change in macromolecular structure.

In addition to desired cure enhancement, the epoxy–amine reaction in the presence of free-radical species may be influenced by side reactions between primary amines and alkenes via a Michael's addition (MiA) mechanism.[14] The amine product formed by the MiA reaction (Fig. 4) will result in unreacted epoxy in the final network and an uncontrollable decrease in crosslink density. Incomplete reactions of the epoxy network will have a deleterious effect on the resulting thermomechanical properties of the SeqIPN. Thus, EA polymerization conditions must be selected carefully to minimize the extent of MiA side reactions. Previous researchers[3] demonstrated that the MiA reaction of a primary amine follows the traditional reactivity rate for unsaturated carbon bonds where

$$\text{allyl} \gg \text{acryl} > \text{methacryl} \gg \text{disubstituted}$$

Dalal and Palmese[15] characterized the reaction rate (k) between a primary amine with epoxide (EA), acrylate (AA), and methacrylate (MA) functionalities and determined $k_{EA} > k_{AA} > k_{MA}$. They also verified that the effective rate of formation of the MiA product is highly temperature dependent. The methacrylates that we selected for this study are less reactive than are allyl and acrylate moieties. Nevertheless, reaction conditions for EA polymerization are selected to minimize the potential side reactions. FTIR cure studies were performed to assess the rate of reaction and extent of conversion of epoxy–amine, as well as the extent of MiA side reactions that occur as a function of temperature.

Methacrylate Network Formation

Once reacted, the epoxy–amine network serves as a template for the ensuing methacrylate network formation via free-radical polymerization. Typical homopolymerization of methacrylates produces a high degree of shrinkage (8–12%) on curing. One effect of polymerizing the methacrylates on the EA template is reduced cure shrinkage (2–4%) in the SeqIPNs.

To compare thermally cured samples with e-beam–processed SeqIPNs, we sought to form the thermal initiated methacrylate networks after EA formation was completed. Therefore, we selected a high-temperature initiator, di-tert-butyl peroxide (1-h $T_{1/2}$ = 149°C) for the free-radical cure of methacrylates. The dimethacrylate network is thermally cured at 180°C for 24 h. For the e-beam–initiated systems, no peroxide initiator is required because e-beam irradiation induces high concentrations of radicals within the matrix on exposure.[16] E-beam MA cure is achieved using 10 MeV electrons applied to a total dose of 20 Mrad (200 kGy) with a step-cure profile of 6 passes (1 Mrad, 2 × 2 Mrad, 3 × 5 Mrad), performed at E-Beam Services (Cranbury, NJ). The initial dose is small to prevent overheating of the specimens. Note that e-beam cure is performed on C-staged SeqIPNs. Figure 5 shows the FTIR intensity versus wavenumber for the unsaturated carbon-carbon stretching region (1700–1500 cm^{-1}). Evaluation of initial versus final intensity of the peak at 1637 cm^{-1} demonstrates that the extent of conversion in both e-beam and thermal cured samples is equivalently high (>87%), for both the toughened (I01E and I01T) and untoughened (I00E and I00T) samples, with either thermal or e-beam cure. The two cure methods appear to produce similar molecular networks in the IPNs.

Table III Extent of Epoxide Conversion with Time and Temperature for Epoxy–Amine Network Formation in SeqIPN (S) and Model (M) Systems

Cure Temperature (°C)	Epoxide Conversion					
	100 min		300 min		1000 min	
	S	M	S	M	S	M
30	36		67		92	
50	64	59	85	66	95	67
65	79		95		98	
80	92	68	99	70	—	—

Regardless of the processing method, the methacrylate network is formed by free-radical propagation. However, because of the difference in the initiating conditions between thermal and e-beam techniques, mechanical differences may exist between the networks. In addition, the reactivity of the internetwork crosslink sites to the two initiation mechanisms may result in structural differences between the thermally cured and e-beam–cured SeqIPNs.

RESULTS AND DISCUSSION

Kinetics

The characteristic vibrational bands of epoxide, amine, and methacrylate species were monitored at 30, 50, 65, and 80°C to determine the extent of epoxide conversion (p) (see Table III). The extent of MiA side-reaction contributions was also monitored. The extent of conversion was determined using

$$p = \frac{\dfrac{A_x(t=0)}{A_r(t=0)} - \dfrac{A_x(t)}{A_r(t)}}{\dfrac{A_x(t=0)}{A_r(t=0)}} \qquad (1)$$

where A is absorbance, x is the characteristic absorbance frequency, and r is the normalized reference. Figure 6 displays FTIR intensity versus wavenumber for the amine/hydroxyl conversion (4000–2500 cm^{-1}) and epoxide reduction (1100–800 cm^{-1}) before and after reaction with PACM. The formation of strong hydroxyl stretching modes and the reduction in the amine hydrogen intensity provide qualitative evidence of the EA reaction progress. However, the epoxide stretching is used to quantify chemical conversion in the SeqIPNs.

The conversion of epoxide as a function of cure time at incremental cure temperatures is shown in Figure 7 for ETBN-modified SeqIPNs and model systems (I01T and E01T). Differences between the cure behavior of the two systems are apparent. The polymerization rate and degree of conversion in the model system (E01T) show the expected dependence on the cure temperature (T_c) because the polymer network vitrifies prior to complete reaction. Therefore, the cure conversion in the model EA networks at 50 and 80°C is incomplete. A higher degree of polymerization can be achieved, but only by raising the temperature above the initial isothermal T_c. Consequently, the cure profiles for the model system represent the extent of reaction until vitrification. In contrast,

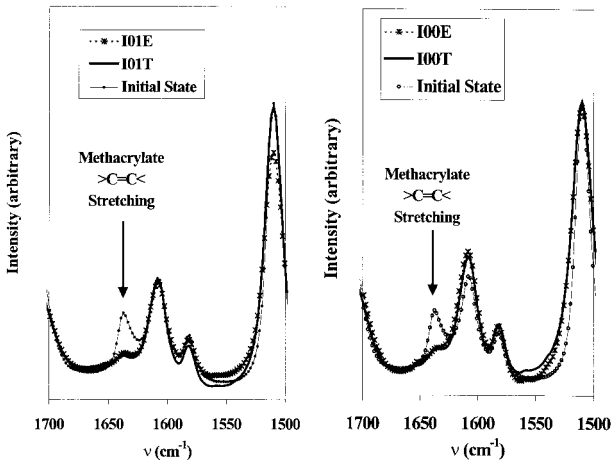

Figure 5 FTIR spectral intensity for the methacrylate region at initial (uncured) and final cure for both thermal (I00T and I01T) and e-beam (I00E and I01E) processed SeqIPNs. The extent of MA conversion is 87% for both cure methods.

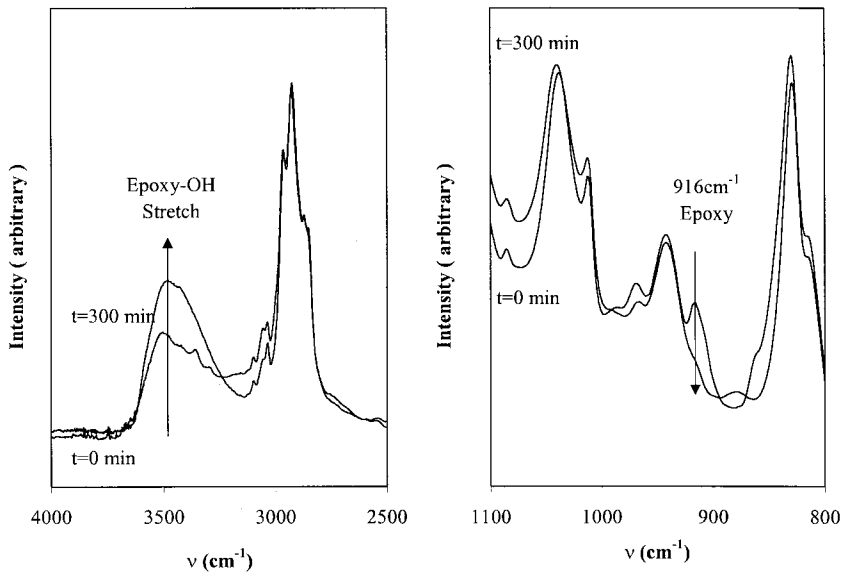

Figure 6 FTIR spectra of SeqIPN formation for I00T before (t = 0 min) and after (t = 300 min) reaction at 80°C. Development of hydroxyl stretch (~ 3400 cm^{-1}) and elimination of epoxide stretch (916 cm^{-1}) is evidence for complete cure conversion.

the SeqIPNs cured under identical isothermal cure conditions (50 and 80°C) achieve complete conversion as a result of the dilution effect of the methacrylates. The vitrification temperature for the SeqIPNs appears to be between 30 and 50°C. Indeed, DSC measurements indicate a broad glass-transition temperature centered at 36°C for the epoxy–amine matrix of the SeqIPNs.

Comparing the initial polymerization ($p < 0.5$) of the model and SeqIPN networks gives insight into the polymerization mechanisms. The intrinsic polymerization rate for the formation of EA is measured using FTIR at a number of cure temperatures. At low conversions ($p < 0.5$), a first-order rate dependence can be assumed for both the model and SeqIPN networks, and eq. (2) can be used to determine the kinetic constants for epoxide conversion versus time.

$$p = 1 - Ae^{-kt} \tag{2}$$

Equation (2) is valid for low degrees of conversion of monomer, where the effects of increasing polymer molecular weight and solution viscosity are negligible. Flory[17] presented stochastic argu-

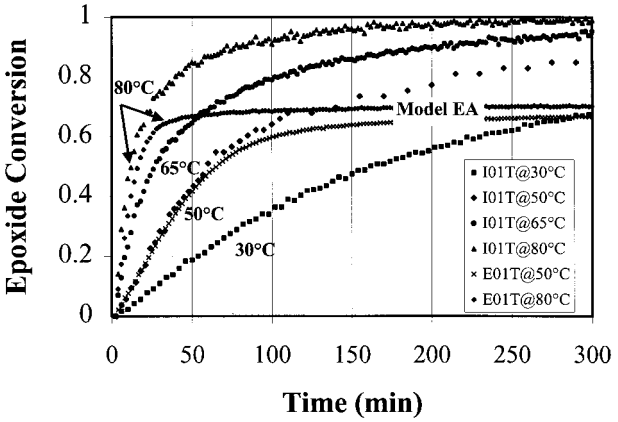

Figure 7 Epoxide conversion versus cure time for ETBN-modified EA in SeqIPNs and model epoxy–amine networks at various cure temperatures.

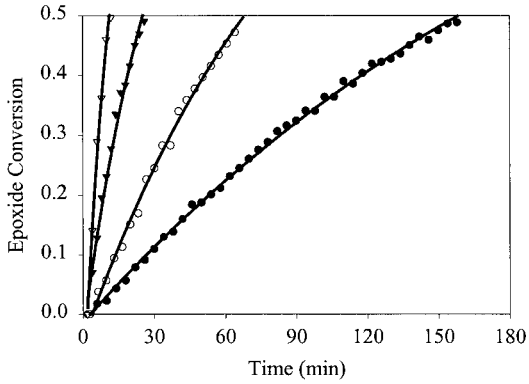

Figure 8 First-order kinetic fits for polymerization of epoxide with amine to p = 0.5 for SeqIPNs at 30, 50, 65, and 80°C.

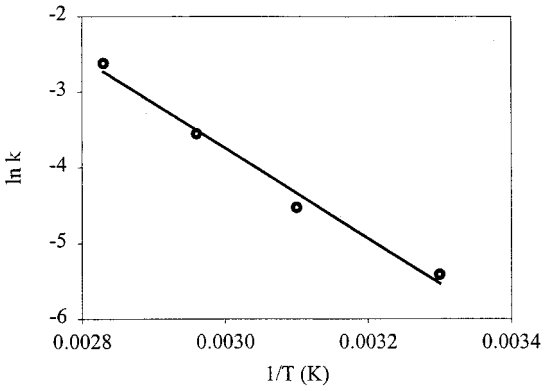

Figure 9 Arrhenius plot for kinetics parameters from first-order polymerization of SeqIPNs to form EA networks. E_a is 49.5 kJ/mol.

ments for build-up of MW and gelation in highly crosslinked networks as a function of the monomer functionality [$f = 1 - (1/\alpha)$] and showed theoretically and experimentally that network viscosity becomes infinite near gelation. Here α is the branching coefficient as defined by Flory. For the present case ($f = 4$), gelation occurs theoretically at $\alpha_{gel} = 0.33$ or $p = 0.57$ ($p^2 = \alpha$). However, because of the composition (25% internetwork crosslinks), the effective branching coefficient retards the onset of gelation and $p = 0.66$ for the SeqIPNs. Therefore, to avoid introducing effects associated with diffusion and gelation, the temperature-dependent polymerization rate constants (k) are obtained by fitting eq. (2) to $0 < p < 0.5$. The fits for SeqIPN formation are shown in Figure 8.

The temperature-independent activation energy (E_a) can be calculated by the Arrhenius approach, which involves a best fit of the ln(k) versus inverse temperature (Fig. 9). The intrinsic activation energy for EA network formation is determined to be 49.5 kJ/mol for the SeqIPNs, whereas the model EA network is 48 kJ/mol. Previously, Sanford[18] evaluated a similar DGEBA–PACM blend and measured an activation energy of 53.5 kJ/mol, in qualitative agreement with our results. Consequently, the polymerization mechanisms for formation of EA networks in SeqIPNs and the model systems are identical, which would imply that the dimethacrylates behave as an inert diluent. Varying the concentration of methacrylates also produced no measurable change in the activation energies. In addition, the methacrylate concentration measured by FTIR remains constant throughout the experimental ranges evaluated. We conclude that MiA side reactions are insignificant to the network structure in the SeqIPN materials. Therefore, the coupling between the two networks of the SeqIPNs occurs entirely through the bifunctional monomers.

Structure

IPNs are frequently observed to phase- or microphase-separate during polymerization and the resulting morphology of the IPN greatly influences material properties. The order of the reactions, their rate, and the miscibility of the two networks with one another lead to a number of interesting multiphase morphologies and properties. Although the SeqIPNs are optically transparent, microphase separation may still occur and explain the thermomechanical behavior of the SeqIPNs. The effectiveness of the elastomer addition on toughening these SeqIPNs is expected to be very dependent on the size, volume fraction, and spacing of the phase-separated rubber-rich domains in the modified SeqIPN materials. Macroscopic phase separation did occur, as reported in Figure 2, and the detailed morphology in these elastomer-modified systems should be examined.

The dimethacrylate and epoxy–amine monomers that we studied form brittle matrices when

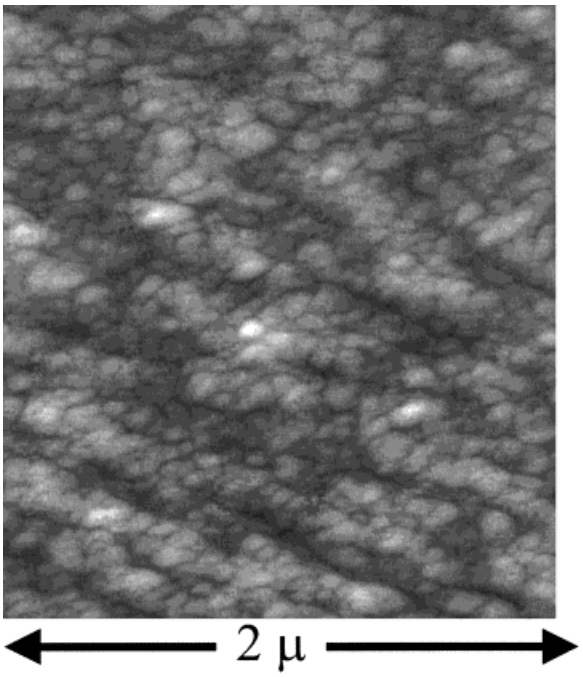

Figure 10 Microphase structure in unmodified epoxy–methacrylate SeqIPN structure as revealed by AFM (contrast enhanced).

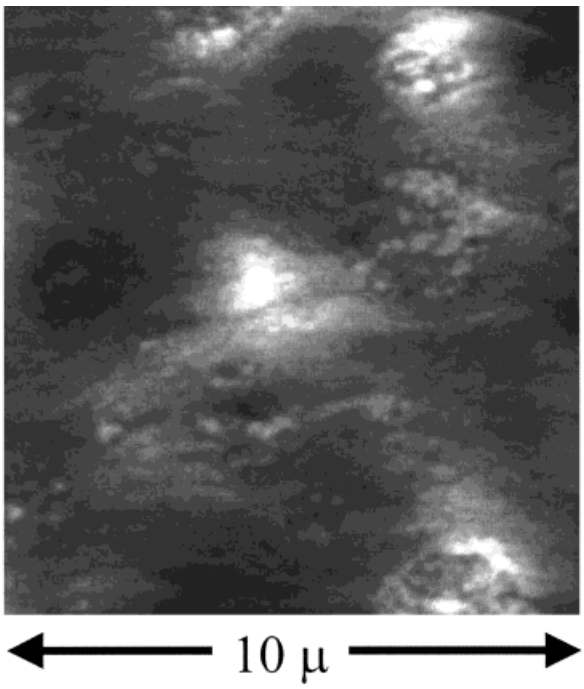

Figure 11 AFM image of a fracture surface for an e-beam–cured rubber-toughened (I01E) SeqIPN with two-phase macrostructure (contrast enhanced).

homopolymerized independently. However, when these two polymer networks are synthesized together as SeqIPNs, the toughness improves even in the absence of a rubber toughener. The SeqIPNs in this work have nearly double the toughness observed for that of DGEBA–PACM and MDGEBA alone.[19] The increase of toughness may be attributed to the microphase morphology that is produced during the two-stage polymerization of the networks. Figure 10 shows a tapping-mode AFM image of the SeqIPN microstructure for the thermally cured SeqIPN (I00T). The cocontinuous microphase morphology is consistent with traditional IPNs that were examined using transmission electron microscopy (TEM).[1] The small domain sizes permit significant interactions between the two network structures and may result in the observed increase in toughness while concomitantly preserving the thermomechanical properties.

The addition of elastomers to the SeqIPN material results in macrophase separation of rubber-rich domains from the SeqIPN matrix, as indicated in the phase diagram of Figure 2. The phase separation occurs during the formation of the EA network, and persists after e-beam or thermal processing to form the second network. The phase diagram determined from turbidity measurements showed that phase separation of ETBN occurred for a range of compositions (Fig. 2). The phase-separated morphology for these materials was evaluated using both AFM and SEM to look at fractured surfaces of the SeqIPNs. Figure 11 shows the tapping mode AFM image of phase-separated rubber regions in the continuous matrix for a typical SeqIPN containing 10% ETBN (I01T). The size of the rubber domains is approximately 1.5–2.0 μm, slightly larger than those observed for the same rubber concentration in the model systems. Some fine structure is also evident within the ETBN phase, which is not fully characterized at this time. Additional studies are currently under way to elucidate the source of structure within the elastomer domains. A complementary SEM micrograph of an ETBN-modified SeqIPN is shown in Figure 12. The ETBN concentration is 5% for this image. On fracture, the rubber particles provide stress-concentration zones for matrix yielding and rubber cavitation. The cavitation around each of the particles supports previously proposed mechanisms for enhanced toughness observed in elastomer-modified thermosets.[20] Thus, the SEM provides physical evidence of improved energy absorption during the fracture process, a phenomenon that is consistent with our observations that elastomer-modified SeqIPNs possess higher fracture toughness.[21]

Thermal Analysis

Dynamic mechanical analysis of multicomponent interpenetrating networks has been used to ex-

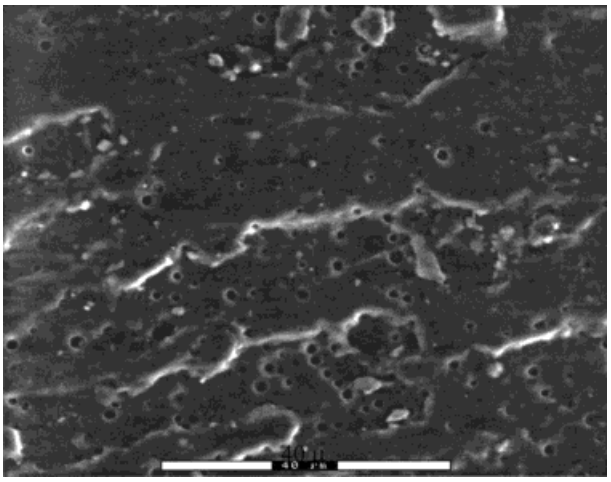

Figure 12 SEM image (×1100) of a fracture surface for an e-beam–cured rubber-toughened (I01E) SeqIPN with two-phase macrostructure (contrast enhanced).

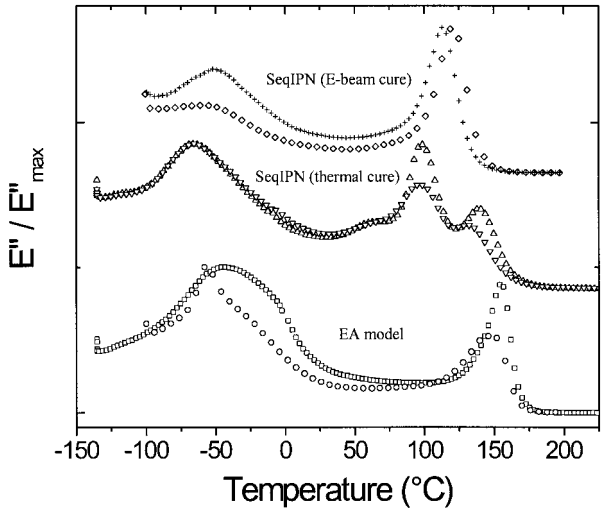

Figure 13 Dynamic loss modulus curves for neat (□) and rubber-toughened (○) EA model, neat (△), and rubber-toughened (▽) thermally cured SeqIPN resins, and neat (◇) and rubber-toughened (+) e-beam–cured SeqIPN resins.

amine the level of compatibility between the various network constituents.[22–25] Typically, highly miscible IPNs have been shown to exhibit a single T_g, whereas phase-separated IPNs display two distinct glass transitions. Figure 13 illustrates the dynamic E'' curves for both the thermally cured and the e-beam–cured neat and rubber-toughened SeqIPN adhesives, as well as those for the neat and rubber-toughened model epoxy for comparison. The addition of the rubber toughener to the model EA network results in a slight decrease in T_g, from 155 to 147°C. This can also be seen in the DSC scans illustrated in Figure 14. The T_g was taken as the temperature of the peak maximum for the primary α-transition. The shape of the secondary β-relaxation for the rubber-toughened epoxy is also changed in comparison to that of the neat model EA network. The rubber-toughened model EA network displays a new transition at −56°C, which is not evident in the broad secondary β-relaxation of the neat EA network, and is ascribed to phase-separated rubber-rich domains.

The E'' spectra for the thermally cured SeqIPNs reveal the presence of two α-transition peaks for both the neat and rubber-toughened SeqIPN networks. The primary α-transition (α_1 = 140°C) is attributed to the glass transition of the EA network, whereas the secondary α-transition (α_2 = 98°C) is the glass transition of the methacrylate network. Upon the addition of the ETBN rubber toughener, the T_g of the α_2-transition remains nearly unchanged at 96°C. However, the T_g of the α_1-transition in the rubber-toughened SeqIPN decreased slightly to 132°C, which may result from the partial solubility of the elastomer in the EA phase. A single broad glass transition is observed using DSC for the thermally cured SeqIPNs, as seen in Figure 14. The slight decrease of T_g for the EA network upon addition of the ETBN is a good indication that the rubber toughener is experiencing some degree of phase separation in the cured SeqIPN network.[26] However, the evidence of an additional low-temperature E'' peak is absent in the 1-Hz DMA spectra of the rubber-toughened thermally cured SeqIPN. In contrast to the thermally cured SeqIPNs, the e-beam curing method produces a single E'' peak at the α-transition. This single α-relaxation is also confirmed in the DSC plot of Figure 14. The T_g of the e-beam–cured SeqIPN is slightly reduced by the rubber toughener, from 121 to 113°C. The relative magnitude of the secondary β-relaxation is greater for the rubber-toughened e-beam–cured SeqIPN compared to that of the neat counterpart, but the shape of the relaxation peak is similar. The DMA and DSC results are summarized in Table IV.

To probe the low-temperature damping response of all the networks in more detail, multiple-frequency sweeps were performed from −135 to 25°C in 3°C isothermal-temperature increments. Figure 15 illustrates the 0.1-, 1-, and 10-Hz E'' curves of the secondary β-relaxation of the neat and rubber-toughened EA networks. The β-relaxation of the neat EA network encompasses the entire temperature range plotted from −100

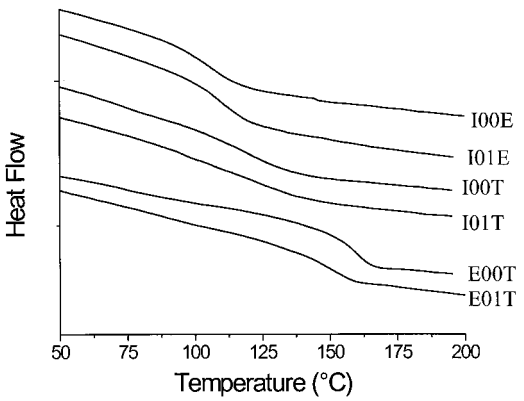

Figure 14 DSC results for SeqIPN (I00E, I01E, I00T, I01T) and model epoxy–amine (E00T and E01T) thermosets on second heat.

Table IV Thermal Characterization Results, WLF Parameters, and KWW Parameters

System	T_g DSC (°C)	T_g DMA (°C)	C_1	C_2 (K)	β	τ^* (s)
I00E	107	121	15.1	77.6	0.218	0.053
I01E	110	113	15.7	76.7	0.210	0.11
I00T	119	α_1 = 140 α_2 = 98	—	—	—	—
I01T	110	α_1 = 132 α_2 = 96	—	—	—	—
E00T	160	155	15.3	74.3	0.203	0.035
E01T	151	147	17.6	73.0	0.168	0.17

to 25°C. A single relaxation peak is evident for the neat EA network, which shifts upward in temperature approximately 30°C as the frequencies of the experiment are swept from 0.1 to 10 Hz. The shapes of the β-relaxation E'' curves for the neat EA network do not change as a function of frequency, indicating that a single relaxation mechanism is responsible for this transition.[27] The primary α-relaxation of the rubber-rich phase in the EA network is seen as the additional E'' peaks near −55°C, which occurs within the temperature range of the β-relaxation of the EA phase. In the glassy state the activation energy (E_a) of a molecular relaxation process can be determined using the Arrhenius relationship between frequency (f) and temperature[28]:

$$\ln\left(\frac{f}{f_0}\right) = -\frac{E_a}{R}\left(\frac{1}{T} - \frac{1}{T_0}\right) \tag{3}$$

where R is the universal gas constant, f_0 is the reference frequency, and T_0 is the reference temperature. The activation energy of the low-temperature β-relaxation of the neat EA network can be calculated by plotting the data taken from Figure 15 as log f versus $1/T$, where T is the temperature of the E'' peak maximum, to yield a result of 68 kJ/mol. This low-activation energy is the product of the nonbackbone chain motions typically found in a β-relaxation.[27] The experimental Arrhenius activation energy calculated for the α-relaxation of the rubber-rich phase of the toughened EA network is 212 kJ/mol, which is significantly greater than the low value of E_a determined for the EA β-relaxation.

Although a rubber peak is not present in the 1-Hz E'' spectra of the thermally cured SeqIPN, as seen in Figure 13, this relaxation could simply be obscured to a great extent by the β-relaxation of the SeqIPN. If the α-relaxation of the ETBN rubber modifier and the β-relaxation of the SeqIPN over-

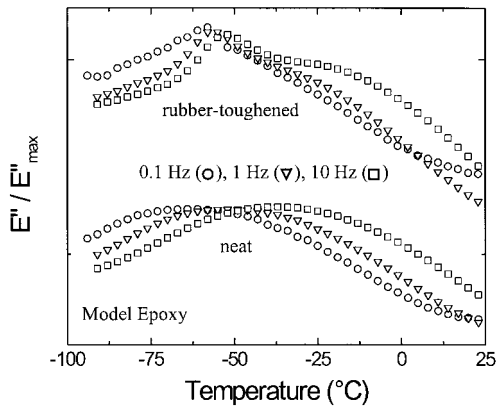

Figure 15 DMA spectra of low-temperature β-transition for the neat and rubber-toughened model epoxies (step isothermal mode).

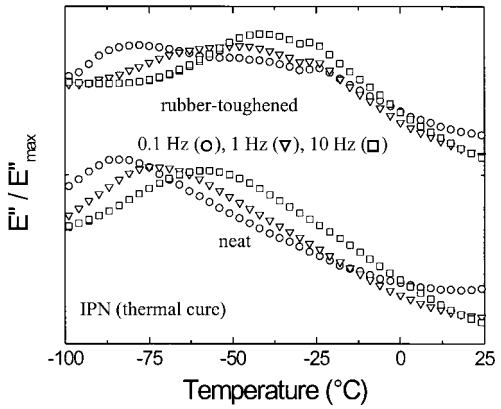

Figure 16 DMA spectra of low-temperature β-transition for the neat (I00T) and rubber-toughened (I01T) thermally cured SeqIPN resins (step isothermal mode).

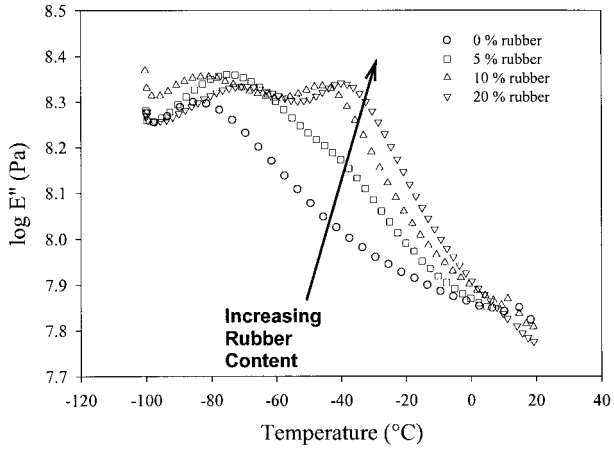

Figure 17 DMA spectra of low-temperature transitions for the e-beam–cured SeqIPN as a function of rubber concentration (0.1 Hz, 2°C/min).

lap, then the two relaxation peaks will shift to differing temperatures as the frequency of the DMA is varied. This was demonstrated in the case of the rubber-toughened EA network. The separation of the peaks occurs as a result of the large differences in activation energies for the β-relaxation of the SeqIPN and α-relaxation of the ETBN elastomer phase. The low-temperature E'' transition as a function of frequency for the neat and rubber-toughened thermally cured SeqIPN is illustrated in Figure 16. The main peak shifts toward lower temperatures as the frequency decreases, whereas a shoulder begins to separate at the high-temperature portion of the curve in the range of -30 to -20°C. The calculated Arrhenius activation energy for the low-temperature E'' peak is 41 kJ/mol, which compares well with E_a equal to 56 kJ/mol for the neat thermally cured SeqIPN. Clearly the β-relaxation of the SeqIPN network is responsible for the main visible low-temperature E'' peak. Therefore, the α-transition of the ETBN rubber toughener must be responsible for the shoulder at the high temperatures of the E'' curve. The high temperature of the α-transition of the ETBN rubber toughener in the SeqIPN systems could be the result of free-radical crosslinking of the carbon–carbon double-bond sites along the backbone chain. Unfortunately, the resolution of the E'' spectra for the rubber-toughened thermally cured SeqIPN was not sharp enough to calculate a value of E_a with a 10% concentration of ETBN. However, as the mass fraction of rubber phase increases, this E'' peak becomes more defined, as seen in Figure 17. Multiple frequency analysis of the e-beam–cured SeqIPN is unsuccessful in resolving the α-transition of the rubber-rich phase and the β-transition of the SeqIPN, as seen in Figure 18, at a rubber concentration of 10%. The values of E_a obtained for the low-temperature transition of the neat and rubber-toughened e-beam–cured SeqIPNs are 80 and 79 kJ/mol, respectively. However, the low-temperature E'' plots portrayed in Figure 17 were obtained from e-beam–cured SeqIPN samples. Therefore, the phase separation of the ETBN rubber must also occur in these systems.

The E'' α-transition of the neat and rubber-toughened thermally cured SeqIPN shows two distinct peaks that result from microphase separation of the methacrylate and EA components of the SeqIPN. The complete miscibility between the individual networks of a SeqIPN is an extremely rare occurrence.[29] The e-beam–cured SeqIPN displays a single E'' peak at the α-transition. This single E'' peak could theoretically result from a nearly perfect overlap of the relaxation times of the EA and methacrylate networks, although multiple-frequency DMA sweeps of the e-beam–cured neat and rubber-toughened SeqIPN samples revealed no peak separation or shoulders as a function of frequency. Time–temperature superpositioning (tTsp) was used to construct master curves of E'' for the model EA networks and e-beam–cured SeqIPN in the frequency domain, to characterize the viscoelastic properties of the glass transition of the e-beam–cured SeqIPN more completely. Assuming a single relaxation mechanism, the distribution of apparent relaxation times (τ^*) as a function of temperature can be described by the empirical Williams–Landel–Ferry (WLF) equation[28]

$$\log a_T = \log \frac{\tau^*}{\tau_R^*} = \frac{-C_1(T - T_R)}{C_2 + (T - T_R)} \tag{4}$$

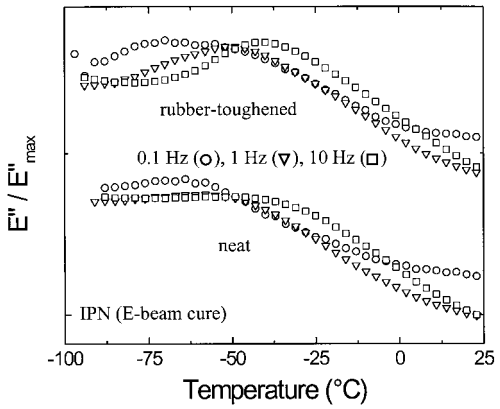

Figure 18 DMA spectra of low-temperature β-transition for the neat (I00E) and rubber-toughened (I01E) e-beam–cured SeqIPN resins (step isothermal mode).

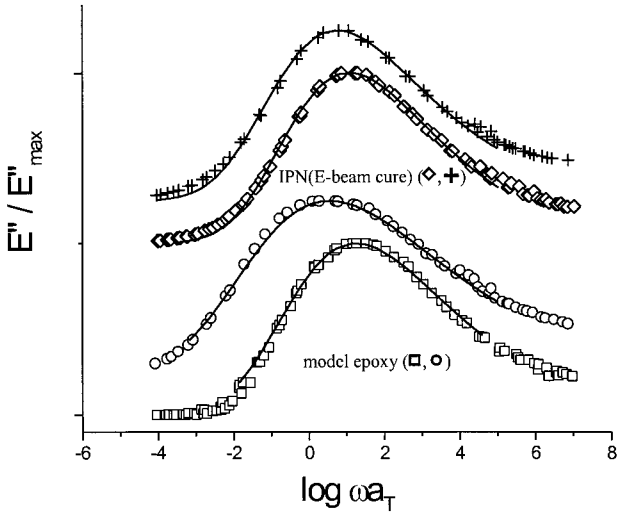

Figure 19 Loss modulus master curves and KWW fits for the model epoxy (□, neat; ○, rubber-toughened) and e-beam–cured SeqIPN (◇, neat; +, rubber-toughened).

where a_T represents the horizontal shift factors obtained when producing the master curve, C_1 and C_2 are constants, and τ_R^* is the apparent relaxation time at a reference temperature T_R. The nonexponential nature of the distribution of relaxation times in polymers can be described by the Kohlrausch–Williams–Watts (KWW) correlation function[30]

$$\phi(t) = \exp\left[-\left(\frac{t}{\tau}\right)^{\beta}\right] \rightarrow 0 < \beta \leq 1 \qquad (5)$$

where β is the stretched exponential function. When $\beta = 1$ the KWW equation describes Debye relaxation. As β decreases the breadth of the distribution of relaxation times increases.[31] The β parameter can be determined using a numerical method to solve the transform of the KWW equation, which was developed by Weiss et al.[32,33]:

$$\frac{E(\omega) - E(\infty)}{E(0) - E(\infty)} = E'(\omega) - iE''(\omega) = -\int_0^{\infty} e^{-i\omega t}\left[\frac{d\phi_\beta(t)}{dt}\right] dt \qquad (6)$$

$$E''(\omega) = AzQ_\beta(z) \qquad (7)$$

$$Q_\beta(z) = \frac{1}{\pi}\int_0^{\infty} e^{-u^\beta}\cos(zu)\, du \qquad (8)$$

where $u = t/\tau$, $z = \omega\tau = 2\pi f\tau$, and A is the normalization factor.

The E'' master curves and least-squares fits to the KWW equation for the neat and rubber-toughened model EA networks and e-beam–cured IPNs are illustrated in Figure 19. The experimental isotherms for each network shifted smoothly to yield a reasonably shaped master curve. The breadth of the rubber-toughened model EA network master curve is slightly broader with respect to frequency than that of the neat EA network. This is reflected in the fits for the β parameter, which were found to be 0.168 ($\tau_R^* = 0.17\ s^{-1}$, $T_R = T_g = 419$ K) and 0.203 ($\tau_R^* = 0.035\ s^{-1}$, $T_R = T_g = 432$ K) for the rubber-toughened and neat-model EA networks, respectively. The breadths of the master curves obtained for the e-beam–cured SeqIPNs are similar for the neat and rubber-toughened samples. The KWW β-fitting parameters calculated for the e-beam–cured IPNs were 0.210 ($\tau_R^* = 0.11\ s^{-1}$, $T_R = T_g = 386$ K) and 0.218 ($\tau_R^* = 0.053\ s^{-1}$, $T_R = T_g = 395$ K) for the rubber-toughened and neat samples, respectively. The WLF and KWW fitting results are summarized in Table IV.

Successful tTsp methods require that the shift-factor plot must appear reasonable.[28] The corresponding shift-factor plots for the rubber-toughened e-beam–cured SeqIPN master curves of Figure 19 are illustrated in Figure 20. The experimental data for the rubber-toughened e-beam–cured SeqIPN ($T > T_g$) were fit to the WLF equa-

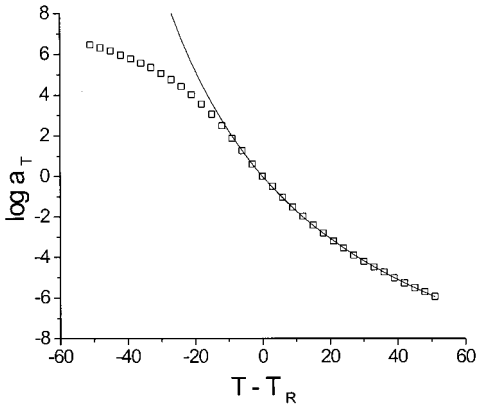

Figure 20 Shift-factor plot and WLF fit for the rubber-toughened e-beam–cured SeqIPN.

tion and are well described by this approach (C_1 = 15.7 K and C_2 = 73.0 K). Similar WLF constants were obtained for the neat e-beam–cured SeqIPN. These values are fairly close to the universal values of 17.4 and 51.6 K.[26] The deviation of the experimental horizontal shift-factor data from the predicted viscoelastic behavior for temperatures $T < T_g$ is attributed to the nonequilibrium glassy state and has been observed by other researchers.[34,35] The tTsp principle is valid only if the shape of the distribution of relaxation times remains unchanged in the frequency or time range of the master curve. Therefore, the α-transition of the e-beam–cured SeqIPNs appears to be the product of a singular relaxation mechanism, which could arise as the result of a high level of coupling between the EA and methacrylate networks. Alternatively, the domain size of any microphase separation between the EA and methacrylate networks of the e-beam–cured SeqIPN could also be too small to be detected by DMA.

CONCLUSIONS

The cure kinetics, structure, and both thermal and viscoelastic properties of SeqIPN networks of epoxy–amine and dimethacrylates were studied for thermal and e-beam processing. The epoxy–amine network is first formed with low-temperature curing to form a swollen gel. The dimethacrylate network is subsequently formed by free-radical polymerization using either thermal initiation by peroxides or direct initiation e-beam. We observed that both thermal and e-beam curing produced high degrees of conversion of methacrylate (indistinguishable by spectroscopic analysis) but that the dynamic mechanical behavior of the networks was different. The thermally cured methacrylate network produced two distinct glass-transition temperatures, whereas the e-beam sample produced a single transition.

The cure mechanisms for forming the EA network were characterized. The polymerization rate for the EA network that formed in the presence of e-beam monomer (diluent) was compared to that of a traditional EA network. The intrinsic polymerization rate and activation energy for formation of the EA networks are identical between the SeqIPN and the model system, implying that the reaction mechanisms are identical and that side reactions between the amine and methacrylate monomers are negligible. The extent of epoxide conversion is higher in the SeqIPN because of the increased mobility in the network brought about by a diluent effect that increases the temperature for the onset of vitrifaction. The observed difference in thermomechanical performance is therefore not related to characteristic molecular structures in the EA network of the SeqIPNs. However, the high degree of epoxide conversion is a key to the modulus retention observed in the DMA.

DMA is the critical characterization technique used to elucidate differences between the thermal and e-beam–cured SeqIPNs. We observed that two high-temperature α-relaxations occur for the thermally processed SeqIPN, whereas only a single α-relaxation occurs in the e-beam–processed SeqIPN. Looking at the construction of the SeqIPNs, we associated this difference with the degree of internetwork coupling. Although spectroscopically we were unable to observe a difference in the e-beam network, the thermomechanical behavior demonstrated a high degree of internetwork coupling, and therefore only one principal relaxation mechanism. The thermally cured SeqIPNs do not achieve the high degree of coupling, so each of the networks in the SeqIPN retain pseudoindependent mobility, producing two relaxations.

The materials characterized in this study are the baseline materials for a new type of e-beam–processible paste adhesives and low-viscosity VARTM resins. E-beam technology has been limited by a lack of performance, particularly with respect to toughness, in e-beam–cured resins. We demonstrated that traditional thermoset toughening could be used to improve toughness in SeqIPN materials, resulting in toughened e-beam resins. The DMA analysis showed that ETBN-modified resins had only slightly reduced glass-transition temperatures, whereas phase-separated rubber domains could be resolved by frequency-modulated DMA. The phase-separated rubber domains are approximately 0.5–2 μm, which is the optimum size range for improving toughness in brittle epoxy resins. Additionally, these phase-separated domains are observed as macrostructures in both AFM and SEM analyses.

The work described in this article was supported by the Strategic Environmental Research and Development Program (SERDP). Additionally, the authors thank Urmish Dalal, Dr. Giuseppe Palmese, Nicholas Sisofo, David Werner, Steven Nguyen, and Susan Fortner for their contributions to the work presented here.

REFERENCES

1. Sperling, L. H. Interpenetrating Polymer Networks and Related Materials; Plenum: New York, 1981.
2. An, J. H.; Sperling, L. H. in Cross-linked Polymers: Chemistry, Properties, and Applications; Dickie, A. A.; Labana, S. S.; Bauer, R. S., Eds.; American Chemical Society: Washington, DC, 1988; p. 269.
3. Dalal, U. P. M.S. Thesis, University of Delaware, 1999.
4. Goodman, D. L.; Palmese, G. R. U.S. Pat. 5,891,292, 1999.
5. Dalal, U. P.; Palmese, G. R. J Polym Sci Polym Chem to appear.
6. Verchere, D.; Pascault, J. P.; Sautereau, H.; Moschiar, S. M.; Riccardi, C. C.; Williams, R. J. J. J Appl Polym Sci 1991, 42, 701.
7. Manzione, L. T.; Gillham, J. K.; McPherson, C. A. J Appl Polym Sci 1981, 26, 889.
8. Williams, R. J. J.; Borrajo, J.; Adabbo, H. E.; Rojas, A. J. in Rubber-Modified Thermoset Resins; Riew, C. K.; Gillham, J. K., Eds.; American Chemical Society: Washington, DC, 1984.
9. An, J. H.; Sperling, L. H. in Cross-linked Polymers: Chemistry, Properties, and Applications; Dickie, A. A.; Labana, S. S.; Bauer, R. S., Eds.; American Chemical Society: Washington DC, 1988; p. 206.
10. Doyle, T. E.; Fekete, F.; Kennan, P. J.; Plant, W. J. U.S. Pat. 3,317,465, 1967.
11. Fitzgerald, J. J.; Landry, C. J. T. J Appl Polym Sci 1990, 40, 1727.
12. Golver, D. J.; Duffy, J. V.; Hartmann, B. J Polym Sci Part A Polym Chem 1988, 26, 79.
13. Hong, S. G.; Wu, C. S. Thermochim Acta 1998, 316, 167.
14. Titier, C.; Pascault, J. P.; Taha, M.; Rozenberg, B. J Polym Sci Part A Polym Chem 1995, 33, 175.
15. Palmese, G. R.; Dalal, U. P. J Polym Sci Part B Polym Phys to appear.
16. Burak, L. J Coat Technol 1997, 69, 29.
17. Flory, P. J. Principles of Polymer Chemistry; Cornell University Press: Ithaca, NY, 1953.
18. Skourlis, T. P. Ph.D. Thesis, University of Delaware, 1996.
19. Sands, J. M.; McKnight, S. H.; Palmese, G. R. Unpublished data.
20. Huang, Y.; Hunston, D. L.; Kinloch, A. J.; Riew, C. K. in Toughened Plastics I; Riew, C. K; Kinloch, A. J., Eds.; American Chemical Society: Washington, DC, 1993.
21. Sands, J. M.; McKnight, S. H.; Fink, B. K. J Adhes to appear.
22. Sung, P. H.; Lin, C. Y. Eur Polym J 1997, 33, 231.
23. Tang, H.; Dong, L.; Zhang, J.; Ding, M.; Feng, Z. Macromol Chem Phys 1996, 197, 543.
24. Li, Y.; Mao, S. J Polym Sci Part A Polym Chem 1996, 34, 2371.
25. Bartolotta, A.; Di Marco, G.; Carini, G.; D'Angelo, G.; Tripodo, G.; Fainleib, A. M.; Slinchenko, E. A.; Shtompel, V. I.; Privalko, V. P. Polym Eng Sci 1999, 39, 549.
26. Aklonis, J. J.; MacKnight, W. J. Introduction to Polymer Viscoelasticity, 2nd ed.; Wiley: New York, 1983.
27. McCrum, N. G.; Read, B. E.; Williams, G. Anelastic and Dielectric Effects in Polymeric Solids; Dover Publications: New York, 1991.
28. Ferry, J. D. Viscoelastic Properties of Polymers, 2nd ed.; Wiley: New York, 1970.
29. Privalko, V. P.; Azarenkov, V. P.; Baibak, A. V.; Korskanov, V. V.; Titov, G. V.; Frisch, H. L.; Zhou, P. Polym Eng Sci 1996, 36, 1052.
30. Williams, G.; Watts, D. C. Trans Faraday Soc 1970, 66, 80.
31. Connolly, M.; Karasz, F.; Trimmer, M. Macromolecules 1995, 28, 1872.
32. Weiss, G. H.; Bendler, J. T.; Dishon, M. J Chem Phys 1985, 83, 1424.
33. Weiss, G. H.; Dishon, M.; Long, A. M.; Bendler, J. T.; Jones, A. A.; Inglefield, P. T.; Bandis, A. Polymer 1994, 35, 1880.
34. Han, Y.; Yang, Y.; Li, B.; Feng, Z. J Appl Polym Sci 1995, 56, 1349.
35. Beckmann, J.; McKenna, G. B.; Landes, B. G.; Bank, D. H.; Bubeck, R. A. Polym Eng Sci 1997, 37, 1459.